Electronic structure and x-ray magnetic circular dichroism of gadolinium beyond the local spin density approximation

Samir Abdelouahed, N. Baadji, and M. Alouani
Institut de Physique et de Chimie des Matériaux de Strasbourg (IPCMS), UMR 7504 CNRS-ULP, 23 rue du Loess, BP 43, 67034 Strasbourg Cedex 2, France

(Received 13 September 2006; revised manuscript received 16 January 2007; published 26 March 2007)

The electronic and magnetic properties of gadolinium are studied by means of the full-potential linear augmented plane-wave method including the Hubbard interaction for describing a $4f$ electron-electron interaction in the mean-field approximation. The manner in which the $4f$ localized orbitals are approximated seems to be of great importance in elucidating the mechanisms responsible for the strong magnetic moment of gadolinium and its ordered magnetic structure as well as the relative energy positions of the occupied and empty $4f$ states. Through various calculations, including the spin-orbit coupling in a second-variation scheme, within the local-spin-density approximation (LSDA), the generalized-gradient approximation (GGA), the LDA+U, and the GGA+U, it is clearly shown that the LDA+U or the GGA+U are the most adequate methods for describing the electronic and magnetic structures as well as the x-ray absorption (XAS) and x-ray magnetic circular dichroism (XMCD) of the the strongly correlated $4f$ electrons of gadolinium. In particular, the calculated $L_{2,3}$ and $M_{4,5}$ XAS and XMCD spectra are found in good agreement with the experimental ones except that the shoulder above the principal peak of the $M_{4,5}$ spectra is not present in the calculation. The spin magnetic moments of the $5d$ states obtained from the XMCD spectra using the XMCD sum rules compare favorably with the self-consistent band-structure results only when the dipole magnetic term is included in the calculation.

DOI: 10.1103/PhysRevB.75.094428 PACS number(s): 71.15.Ap, 71.20.Eh

I. INTRODUCTION

The appropriate treatment of the localized $4f$ electrons in first-principles calculations has been debated since the pioneering work of de Dimmock and Freeman[1] within the augmented plane-wave (APW) framework, dating the birth of the $4f$-core model where the $4f$ states are treated as atomic core states. Since then, many attempts have been made to improve the description of the strongly localized and correlated $4f$ electrons in gadolinium.[2,3] In order to take into account the hybridization of the $4f$ states with the other valence electrons Singh[4] carried out calculations within the $4f$-band model. It showed the importance of the f-electron itineracy in explaining the details of the Fermi surface structure obtained by performing de Haas–van Alphen (dHvA) experiment[5,6] and supported early work by Sticht and Kübler[2] and Temmerman and Sterne.[3] However, Ahuja *et al.*,[7] based on their work by means of the linear muffin-tin orbital method (LMTO) within the atomic sphere approximation (ASA), contradicted this conclusion by showing the possibility of providing a good description of the dHvA experimental results for terbium and gadolinium without the inclusion of the hybridization of the $4f$ states with the other states. Recently, however, Santos, Nolting, and Eyert[8] combined a many-body Kondo lattice model with an *ab initio* band structure calculation to determine self-consistently the Curie temperature and the magnetic moment of metal gadolinium. The results were found in good agreement with the experimental results.

In a recent paper, Kurz *et al.*[9] approached the question of how to treat the $4f$ states in a more systematic manner by performing several types of scalar-relativistic calculations [without spin-orbit coupling (SOC)] using the full-potential linear APW (FLAPW) method as is implemented in the FLEUR code.[10] The calculations were carried out using the $4f$-core model, the $4f$-band model, the "hybrid" model in which the majority $4f$ electrons are treated as valence electrons and the minority $4f$ electrons are *removed* from the valence band region by *shifting* the $4f$ minority band center far above the Fermi energy as in the $4f$-core model, and the LDA+U (Ref. 11) method. They showed that the $4f$-band model, using the local-spin-density approximation (LSDA) or the generalized-gradient approximation (GGA) potentials, produces almost the same results and leads always to an incorrect antiferromagnetic (AFM) ground state contradicting earlier work of Temmerman and Sterne.[3] On the other hand, the $4f$-core model, the hybrid model, or the LDA+U method leads to the correct ferromagnetic (FM) ground state in agreement with the previous results of Shick and co-workers.[12] They assigned this incorrect band-model description by means of the LSDA or the GGA to the overestimated (compared to experiment) $4f$ minority density of states at the vicinity of the Fermi level, giving rise to an unphysical partial occupation of the minority $4f$ states. They concluded that the removal of the minority $4f$ states from the Fermi energy—irrespective of the particular model—leads to a correct description of the magnetic ordering, while the description of other quantities, such as the lattice constants or the magnetic moments, depends sensitively on the exact energy position of the $4f$ states and, therefore, on the type of model used. The earlier hexagonal close-packed ferromagnetic ground state found within the LSDA or the GGA was attributed to errors due to the use of the ASA.

The LDA+U based methods are then of great help in describing the basic electronic structure of localized electrons. This is because the self-interaction correction (SIC)

among the localized $4f$ electrons is removed in this formalism. Explicit self-interaction correction orbital-dependent functionals have been initially developed by Perdew and Zunger[13] and have been fully implemented to describe the localized $4f$ electrons in γ-cerium so that the three Hund's rules are fulfilled.[14] The method was also successfully used to describe the magnetism and insulating behavior of $3d$ metal oxides[15] or rare-earth oxides.[16] In this respect, the LDA+U and LDA+SIC methods are somehow similar since both methods remove the self-interaction from the localized electrons.

In the present paper we extend the previous work of Kurz and co-workers by using the first-principles FLAPW method by including the SOC as implemented in the FLEUR code[10] to show that both the LDA+U and GGA+U provide a better description of the electronic properties of the correlated $4f$ electrons than either the LSDA or the GGA, and are strongly recommended for a precise description of the electronic structure, especially of the relative energy positions of the minority and majority $4f$ states, managed by the intrasite Coulomb interactions of the $4f$ electrons. However, the GGA+U provides a slightly better energy splitting, but this difference can be debated (see Sec. III A). In addition, we show that all approximations used in this study led to similar XAS and XMCD spectra and produced spin moments in good agreement with the self-consistent calculation and experimental results. Thus, our work goes beyond that of Carra and co-workers[17] concerning the study of the x-ray magnetic circular diachroism (XMCD) of gadolinium.

Our paper is organized as follows. In the Sec. II we provide some details about our method of calculation and give some useful parameters used in the calculations of the ground state of gadolinium. In the Sec. III we discuss the electronic structure of gadolinium and its Fermi surface with the different potential approximations (LSDA, GGA, LDA+U, and GGA+U) and show that the Hubbard interaction is important for the correct description of the magnetic order and the experimental photoemission for the occupied states and bremsstrahlung isochromat spectroscopy (BIS) for the unoccupied states. A discussion of the various models of how to treat the $4f$ electrons will be also given. In the Sec. IV we provide our results concerning the x-ray absorption and x-ray magnetic dichroism at the L_2, L_3, and $M_{4,5}$ edges of gadolinium and compare them to the experimental data. We show also our magnetic moments calculations using the XMCD sum rules and compare them to the direct self-consistent calculation. In the last section we summarize our paper.

II. COMPUTATIONAL DETAILS

We have used the FLAPW method[19,18] as implemented in the FLEUR code[10] including the SOC to describe the x-ray absorption spectra (XAS) and XMCD at the $L_{2,3}$ and $M_{4,5}$ edges of gadolinium. For the exchange and correlation potential we used both the Moruzzi-Janak-Williams (MJW) parametrization[20] and the GGA of Perdew, Burke, and Ernzerhof.[21] As for the rotationally invariant LDA(GGA)+U methods used in this study, they are similar to the implementation of Shick *et al.*[11] We have to solve the LDA(GGA)+U using the full Hamiltonian and not the second-variational method.[11] The LDA(GGA)+U Schrödinger equation can be derived from the variational principle and is given by[11]

$$[-\nabla^2 + V^{\sigma}(\mathbf{r})]|\Psi_n^{\mathbf{k},\sigma}\rangle \tag{1}$$

$$+\sum_{t,m,m'}\left[|\phi_{t,\ell m}\rangle V^{t,\ell,\sigma}_{m,m'}\langle\phi^{\sigma}_{t,\ell m'}|\Psi_n^{\mathbf{k},\sigma}\rangle + \frac{|\dot{\phi}^{\sigma}_{t,\ell m}\rangle V^{t,\ell\sigma}_{m,m'}\langle\dot{\phi}^{\sigma}_{t,\ell m'}|\Psi_n^{\mathbf{k},\sigma}\rangle}{\langle\dot{\phi}^{\sigma}_{\ell m}|\dot{\phi}^{\sigma}_{\ell m}\rangle}\right] = E_n^{\mathbf{k},\sigma}|\Psi_n^{\mathbf{k},\sigma}\rangle, \tag{2}$$

where

$$\begin{aligned} V^{t,\ell\sigma}_{m_1,m_2} = &\sum_{m_3,m_4}\langle\phi_{t,\ell m_1};\phi_{t,\ell m_3}|V_{ee}|\phi_{t,\ell m_2};\phi_{t,\ell m_4}\rangle n^{t,-\sigma}_{m_3,m_4} \\ &+\sum_{m_3,m_4}[\langle\phi_{t,\ell m_1};\phi_{t,\ell m_3}|V_{ee}|\phi_{t,\ell m_2};\phi_{t,\ell m_4}\rangle \\ &-\langle\phi_{t,\ell m_1};\phi_{t,\ell m_3}|V_{ee}|\phi_{t,\ell m_4};\phi_{t,\ell m_2}\rangle]n^{t,\sigma}_{m_3,m_4} \\ &-\sum_{\sigma'}\left[U\left(N^{t,\sigma'}-\frac{1}{2}\delta_{\sigma,\sigma'}\right)-\delta_{\sigma,\sigma'}J \right. \\ &\left.\times\left(N^{t,\sigma'}-\frac{1}{2}\right)\right]\delta_{m_1,m_2}, \end{aligned} \tag{3}$$

where V^{σ} is the LSDA or GGA potential calculated using the LDA(GGA)+U charge density, $E_n^{\mathbf{k},\sigma}$ the eigenvalues for the band index n, Brillouin zone $\mathbf{k}$ point, and spin σ. The index t runs over all correlated atoms in the unit cell of the material, ℓ stands for the angular momentum quantum number of the correlated orbital and m the magnetic quantum number, whereas $|\phi^{\sigma}_{\ell,m}\rangle$ is the partial wave of that orbital and $|\dot{\phi}^{\sigma}_{\ell,m}\rangle$ its energy derivative. The matrix elements of the screened Coulomb interaction between two electrons $v_{ee}(\mathbf{r},\mathbf{r}')$ are calculated using the screened Slater integrals F^{ℓ} and the Gaunt coefficients $\langle\ell_1,m_1|Y_{\ell,m}|\ell_2,m_2\rangle$. Thus, these four-center integrals are defined as[11,22,23]

$$\begin{aligned} &\langle\phi_{t,\ell m_1};\phi_{t,\ell m_3}|V_{ee}|\phi_{t,\ell m_2};\phi_{t,\ell m_4}\rangle \\ &\quad=\sum_{\ell=0}^{\infty}\frac{4\pi}{2\ell+1}\sum_{m=-\ell}^{+\ell}\langle\ell_1,m_1|Y_{\ell,m}|\ell_2,m_2\rangle\langle\ell_3,m_3|Y^{*}_{\ell,m}|\ell_4,m_4\rangle F^{\ell}. \end{aligned} \tag{4}$$

The parameters U and J are given by the averages of the Coulomb and exchange integrals, which are related to the Slater integrals F^0, F^2, and F^4 by the properties of Clebsch-Gordan coefficients:

$$U=\frac{1}{(2\ell+1)^2}\sum_{m,m'}\langle\phi_{t,m};\phi_{t,m'}|V_{ee}|\phi_{t,m};\phi_{t,m'}\rangle = F^0, \tag{5}$$

$$J = \frac{1}{(2\ell)(2\ell+1)} \sum_{m \neq m', m'} \langle \phi_{t,m}; \phi_{t,m'} | V_{ee} | \phi_{t,m'}; \phi_{t,m} \rangle = (F^2 + F^4)/14. \quad (6)$$

The localized f orbitals are described by an atomic f-wave function $\phi_{t,3,m}(\mathbf{r}) = \phi_{t,3}(|\mathbf{r}-\mathbf{R}_t|) Y_{3,m}(\mathbf{r}-\hat{\mathbf{R}}_t)$, where $Y_{3,m}$ are the spherical harmonics for $\ell=3$ calculated at the position $\mathbf{R}_t$ of atom t. Because it is difficult to determine the correct dielectric function which is responsible for the screening of the Coulomb interaction of the $4f$ orbitals, the strength of the Hubbard (U) and the exchange (J) interactions are not known. Nevertheless, the *ad hoc* constrained LSDA calculation is often used to compute them.[24] This latter procedure is, however, not based on solid grounds and often leads to values of Hubbard interactions that are under or overestimated to tackle the problem at hand.[24] Here, we have chosen to take the Hubbard interaction U as a realistic adjustable parameter that provides the best agreement with experimental photoemission and BIS. Therefore, we adopt the general form for the four-center integrals, given by Eqs. (4)–(6), as function of U and J, and determine the values that fit best the experimental data. Because the results are fairly insensitive to the exchange parameter J, we have adopted $J=0.7$ eV as in Ref. 9. We have found that this value of $U=7.7$ eV, which is 1 eV larger than that of the latest LDA+U calculations,[9,11,12] is the most appropriate for gadolinium, because it provided the correct energy difference between the energy position of the spin-up and spin-down $4f$ levels.

The SOC is used in the so-called second-variational scheme, where one has first to determine the Kohn-Sham eigenvalues by diagonalizing the scalar-relativistic Hamiltonian H_0 that includes only the Darwin and mass-velocity relativistic terms. The matrix elements of the full Hamiltonian to diagonalize are given by

$$\langle n, \mathbf{k}, \sigma | H | n', \mathbf{k}, \sigma' \rangle = \varepsilon_{n,\mathbf{k}} \delta_{n,n'} \delta_{\sigma,\sigma'} + \langle n, \mathbf{k}, \sigma | H_{SOC} | n', \mathbf{k}, \sigma' \rangle, \quad (7)$$

where the eigenvalues $\varepsilon_{n,\mathbf{k}}$ are obtained by first diagonalizing the Hamiltonian H_0. The spin-orbit Hamiltonian H_{SOC} is determined along the quantification axis $\mathbf{u}$ defined by its polar angles ϑ and ϕ, and is given by

$$H_{SOC} = \xi(r)(\boldsymbol{\sigma} \cdot \mathbf{L})_{\mathbf{u}}, \quad (8)$$

where $\xi(r) = \frac{1}{2m^2c^2r}\frac{dV}{dr}$ and $(\boldsymbol{\sigma}\cdot\mathbf{L})_{\mathbf{u}}$ is given in terms of the spin rotation matrix R by

$$(\boldsymbol{\sigma} \cdot \mathbf{L})_{\mathbf{u}} = \begin{pmatrix} L_z & L_- \\ L_+ & -L_z \end{pmatrix}_{\mathbf{u}} = \left[R(\vartheta,\varphi) \begin{pmatrix} L_z & L_- \\ L_+ & -L_z \end{pmatrix} R^{\dagger}(\vartheta,\varphi) \right]_{\mathbf{z}}, \quad (9)$$

where the spin rotation matrix is given by

$$R(\vartheta,\varphi) = \begin{pmatrix} \cos\frac{\vartheta}{2} e^{-i\frac{\varphi}{2}} & \sin\frac{\vartheta}{2} e^{i\frac{\varphi}{2}} \\ -\sin\frac{\vartheta}{2} e^{-i\frac{\varphi}{2}} & \cos\frac{\vartheta}{2} e^{i\frac{\varphi}{2}} \end{pmatrix}. \quad (10)$$

The diagonalization of the full Hamiltonian, produces the eigenvalues and the eigenvectors as a linear combination of the Bloch wave functions of H_0.

The calculations are performed at the experimental c/a ratio of 1.597 and lattice constant a of 6.858 a.u.[25] The plane-wave cutoff for the basis functions $K_{max}=3.0$ a.u.$^{-1}$, the charge density and potential cutoff $G_{max}=9.0$ a.u.$^{-1}$, the muffin-tin radii $R_{mt}=2.80$ a.u. within which the wave functions as well as the density and the potential were expanded up to $l_{max}=8$ as in Ref. 9. For the Brillouin-zone integration we have used the tetrahedron method[26] and up to 1372 $\boldsymbol{k}$ points in the irreducible Brillouin zone (IBZ) to achieve convergence of the total energy and the eigenvalues to within 1 mRy. For a better description of the shallow core states we have treated the $5s$ and $5p$ semicore states as valence states using local orbitals.[27] Whenever it is not explicitly stated the calculations have been carried out using the GGA+U including the SOC.

III. ELECTRONIC STRUCTURE

During the last decade, first-principles calculations within the LDA(GGA)+U methods have provided a good description and allowed a better understanding of the electronic properties of strongly correlated $4f$ electron materials and Mott-Hubbard insulators. In this section we present results of LDA(GGA)+U calculations. The choice of the J value of 0.7 eV is justified by the early electronic properties study of Harmon and Freeman,[28] within the APW method. They evaluated the strength of the $4f$-conduction-electron exchange interaction inside the muffin-tin spheres for the $4f$-$6s$ and $4f$-$5d$, and they obtained $J_{4f\text{-}5d}$ of 0.5 eV and a $J_{4f\text{-}6s}$ of 0.2 eV and hence a total J of 0.7 eV. As stated in the previous section, the value of the Hubbard interaction U is much more difficult to estimate, because the constrained LSDA calculation does not necessarily provide the ultimate value to be used in an LDA+U or GGA+U study. It is interesting to notice that a value of U larger by 1 eV than the constrained one produced the experimental splitting between the spin up and spin down of the $4f$ energy levels. However, to compare with the XPS and BIS data, we had to rigidly shift the occupied and empty densities of states (DOS) by 1.7 eV towards higher energies.

A. Density of states

Figures 1 and 2 present our LDA+U and GGA+U total DOS calculations, which are in good agreement with the XPS and BIS experimental results,[29] after a rigid shift of the occupied and empty densities of states by 1.7 eV towards higher energies.

The large calculated exchange spin splitting Δ of 11.97 eV obtained using the LDA+U potential and that of 12.2 eV using the GGA+U potential are a direct conse-

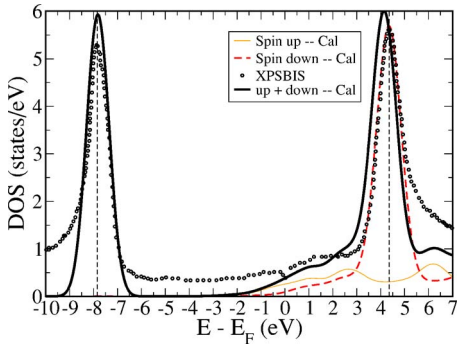

FIG. 1. (Color online) LDA+U total DOS: the orange (thin gray) curve is the spin-up part, the dashed red (dashed black) curve is the spin-down part, and the thick black curve is the sum of the up and down parts as compared to the XPS and BIS experimental data (dotted black curve) of Ref. 29. The calculated spectra are rigidly shifted towards higher energies by 1.7 eV to facilitate the comparison with experiment. The DOS broadened using a full width at half maximum Gaussian smearing of 0.25 eV.

quence of the U effect of 7.7 eV. The angular ℓ resolved DOS (not presented here) showed that the pronounced peaks of the total DOS presented above are almost of f character. In comparing our LDA (GGA)+U DOS with those of the LSDA (GGA), calculated and reported in many recent papers[9,11,12] but not reported here, we noticed that the minority (spin-down) $4f$ states are shifted away from the Fermi energy to higher energies and the majority (spin-up) $4f$ states are shifted to lower energies giving rise to the experimental exchange spin splitting of $\Delta=12.2$ eV. Although the two methods LDA+U and GGA+U produced a good description of the energy distribution of the electronic states, particularly the energy positions of the minority and majority $4f$ states, the GGA+U result is about 0.2 eV larger, in good agreement with the experimental data. We assign the slight improvement of the GGA+U to the fact that the spin-dependent exchange correlation GGA potential describes a bit better the electron-electron interactions involving the strongly localized and correlated $4f$ electrons. With the *help* of the U interaction, the relative position of the $4f$ majority states with respect to the $4f$ minority states is in a better agreement with experiment, leading to a good exchange $4f$ spin-splitting value. However, we cannot state for certain that the GGA

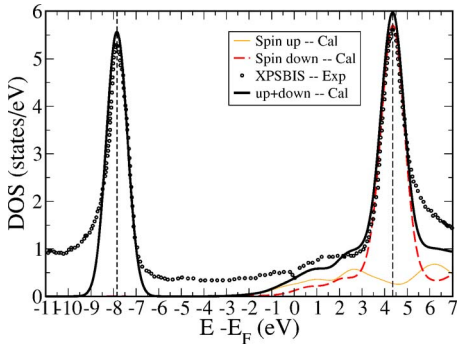

FIG. 2. (Color online) The same as the previous figure but the calculations are done within the GGA+U method.

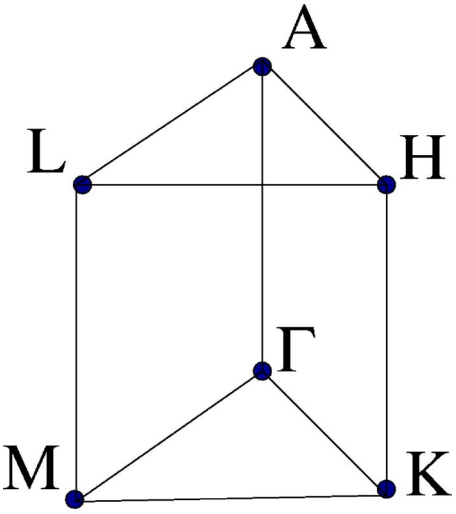

FIG. 3. (Color online) The irreducible part of the hexagonal Brillouin zone.

+U is significantly better than the LDA+U since the small relative accuracy of these two methods can be debated. This is because the DFT error can be much larger than this energy difference.

B. Band structure

Through the band-structure plots reported hereafter, we would like to convey the adequacy of the GGA+U method, compared to the GGA $4f$-core model for the description of the gadolinium electronic structure.

Figure 3 gives the positions of the high-symmetry points in the BZ. Figure 4(a) and 4(b) represent the GGA+U band structure without including the SOC for the majority and minority spin states along high-symmetry directions. The distinguishable dispersionless atomiclike character of the states located at about 2.7 eV above the Fermi level for the minority spin states [Fig. 4(b) and 4(c)] and 9.5 eV below the Fermi level for the majority spin states [Fig. 4(a) and 4(c)] is that of the $4f$ states as is the case experimentally. Despite the crystallographic environment these states behave as in the free atom case due to the fact that the $4f$ electrons are tightly bound to the atom and hence do not overlap appreciably with the neighboring atoms. It is worth mentioning here that the states at the vicinity of the Fermi level are mostly of hybridized $6s$-$5d$ character. The $6s$-band width is larger than that of $5d$ states which is similar to the situation in transition metals, in agreement with the early results reported in Ref. 30. Figure 4(c) shows the effect of the SOC on the GGA+U calculation, in addition to the lifting of the degeneracy for some bands (because the spin is no longer a good quantum number); it is easily seen that the splitting of the $4f$ bands broadened the occupied (majority) bands from 0.2 eV to around 0.8 eV and the unoccupied (minority) bands from 0.3 eV to about almost 0.6 eV. This difference in the splitting of the majority and minority parts can be explained by the large relativistic effects of deep states and the transformation of some $4f$-band character to $6s$- and $5d$-band character via hybridization effects, making the splitting

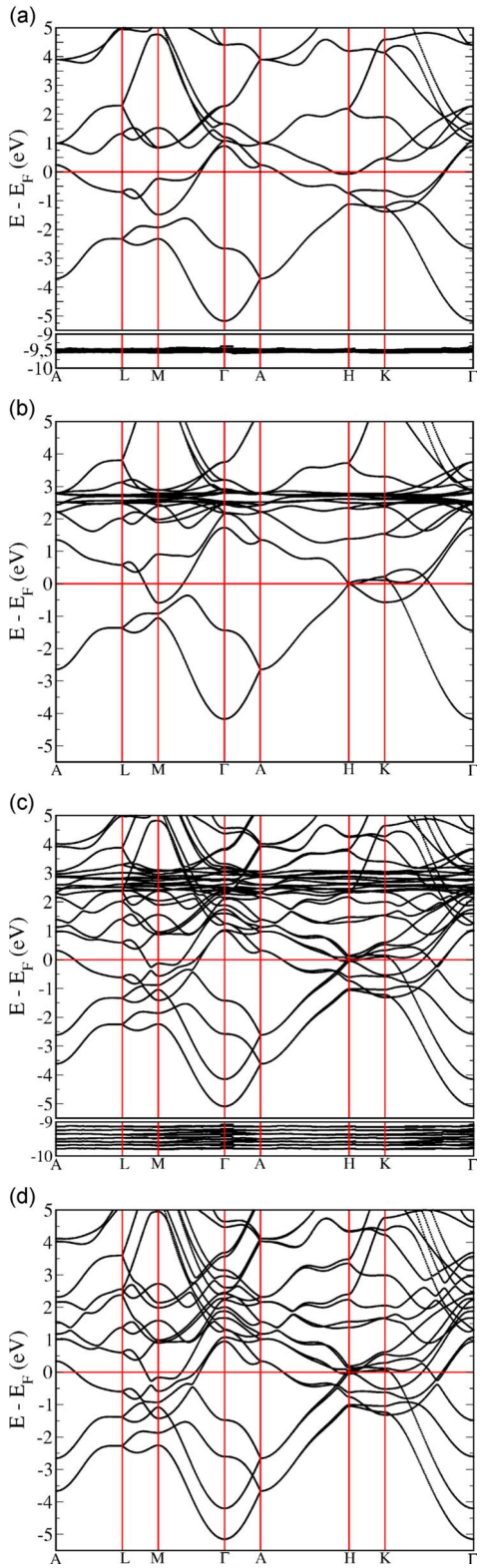

FIG. 4. (Color online) (a) and (b) represent, respectively, the GGA+U band structure plot of the majority and minority spin states without SOC along some high-symmetry directions (see Fig. 3 for the positions of the high-symmetry points in the BZ). (c) represents the total band structure (majority and minority spin states) including the SOC, whereas (d) represents the GGA total band structure (majority and minority spin states), within the 4*f*-core model including the SOC.

mechanism more difficult for the minority electrons than for the majority ones. A part from the effect of splitting, there is no further large effect of the SOC because the 4*f* spin-majority band is fully occupied and the 4*f* spin-minority band is almost completely empty.

To analyze further the hybridization mechanism between the 4*f* states and the 6*s* and 5*d* ones, we report in Fig. 4(d) the SOC 4*f*-core model bands to be compared to the previous SOC GGA+U calculation within the 4*f*-band model. From Fig. 4(c) and 4(d) we can see that the majority 4*f* state removal (in the 4*f*-core model) does not affect the filled states and those lying just above the Fermi level. Hence, the two models provide a similar description for all states lying up to 1 eV above the Fermi energy. However, the minority 4*f* state (located at 2.7 eV) removal affects considerably the surrounding 6*s* and 5*d* bands. In particular, in the 4*f*-core panel of Fig. 4(d), we observe that along the high-symmetry direction *A*-*L*, the band that starts from 2.4 eV at the *A* point and ends at 3.5 eV at the *L* point is almost of 5*d* character. It starts much higher, in the GGA+U 4*f*-model, from 3.1 eV from the *A* point and ends at 3.7 eV at the *L* point. This contraction and small shift of the *s*-*d* bands is ascribed to the hybridization with 4*f* bands. Although the 4*f*-core model removes the unphysical minority 4*f* state contribution to the valence states, it neglects the effects of hybridization of the *f* states with the other states. Therefore, the GGA+U band model produces the experimental energy positions of the 4*f* minority states and reduces their hybridization with the other states, and is more physical than the 4*f*-core model.

It is also worth noting that while the GGA+U or LDA+U methods improved considerably the spin splitting between the spin-up and spin-down 4*f* electrons with respect to the GGA results, it did not affect the spin splitting of the the 5*d*-6*s* bands. This splitting of about 1 eV is found in good agreement with the recent spin- and angle-resolved photoemission result[31] of 0.9 eV. Thus our calculations partially support their conclusion concerning the band structure nature of 5*d*-6*s* states and that the 4*f* correlation does not change the dispersion of these bands below the Fermi level.

It is of great interest to study the Fermi surface of gadolinium using different types of approximations to describe the electron-electron interaction. In Fig. 5 we compare the GGA and GGA+U band structure at the vicinity of the Fermi level along some high-symmetry directions, and in Fig. 6 we plot the three-dimensional representation of the Fermi surface per spin of each band cutting the Fermi level. The calculations are done using the GGA+SOC, GGA, and GGA+U without spin-orbit coupling. The first three rows of (a), (b), and (c) are the majority spin Fermi surfaces of the first three bands cutting the Fermi level, and (d) and (e) are those of minority spins. The total Fermi surface for all bands cutting the Fermi level is represented in the last row (f). To determine the quantitative change of the Fermi surface computed using different *ab initio* methods, we used the linear tetrahedron method to calculate the Fermi surface area of each band. One has to add up over the full BZ the surface areas cutting each tetrahedron for each band crossing the Fermi level. To obtain Fermi surface areas converged to within a relative error of 10^{-4} we used 1372 **k** points in the irreducible BZ. The results of the calculation are displayed in

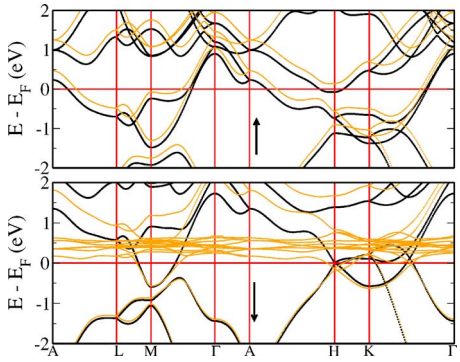

FIG. 5. (Color online) The upper and lower panels represent the comparison of the Gd band structure within the GGA in orange (gray) and GGA+U (black) along some high-symmetry directions (as given by Fig. 3). The spin up is represented in the upper panel and spin down in the lower panel. The Fermi level is at the zero of energy scale.

Table I. Notice that for the calculations including the spin-orbit coupling, the spin is not a good quantum number. Because of the small amount of spin mixing in each Fermi surface, we can still use the spin-up and -down notation. It is interesting to notice that the spin-orbit coupling reduces slightly the areas of all Fermi surfaces, whereas the Hubbard U has a much important effect. First, it reduces also the Fermi surfaces areas of both spin-up and spin-down bands crossing the Fermi level. Second, because of the shifting of the energy bands towards low energies (see Fig. 5), a new electron pocket with a sizable Fermi surface area appeared at the high-symmetry point. We can therefore conclude that both the SOC and the U parameter have an effect on physical properties involving the Fermi surface, like electronic and thermal transport or crystalline magnetic anisotropy. It should be of great interest to study the effect of electron-electron interactions on the dHvA frequencies and masses. We can already say that these frequencies which are proportional to the Fermi surface cross-sectional areas will be reduced when either the SOC or the Hubbard U are included in the calculations.

C. Magnetic order

According to the experimental investigations of Jensen and Macknitosh,[32] it is known that the localized spin moments of gadolinium couple through a Ruderman-Kittel-Kasuya-Yosida- (RKKY) type exchange interaction to form a FM Heisenberg system with a bulk Curie temperature (T_c) of 293 K. In order to discuss the ground-state magnetic configuration of FM gadolinium, we have carried out total-energy first-principles calculations for the FM and AFM configurations. The AFM configuration calculations were done by reversing the magnetization sign of every second close-packed plane of atoms along the c direction. The total-energy differences $\Delta E_{(\uparrow\downarrow-\uparrow\uparrow)}$ between the AFM configuration $\uparrow\downarrow$ and the FM $\uparrow\uparrow$ one, recapitulated in Table II, show that the LDA (GGA)+U favor the experimental FM configuration over the AFM one. These results are in agreement with the calculations of Ref. 9 using the force theorem. Those authors have

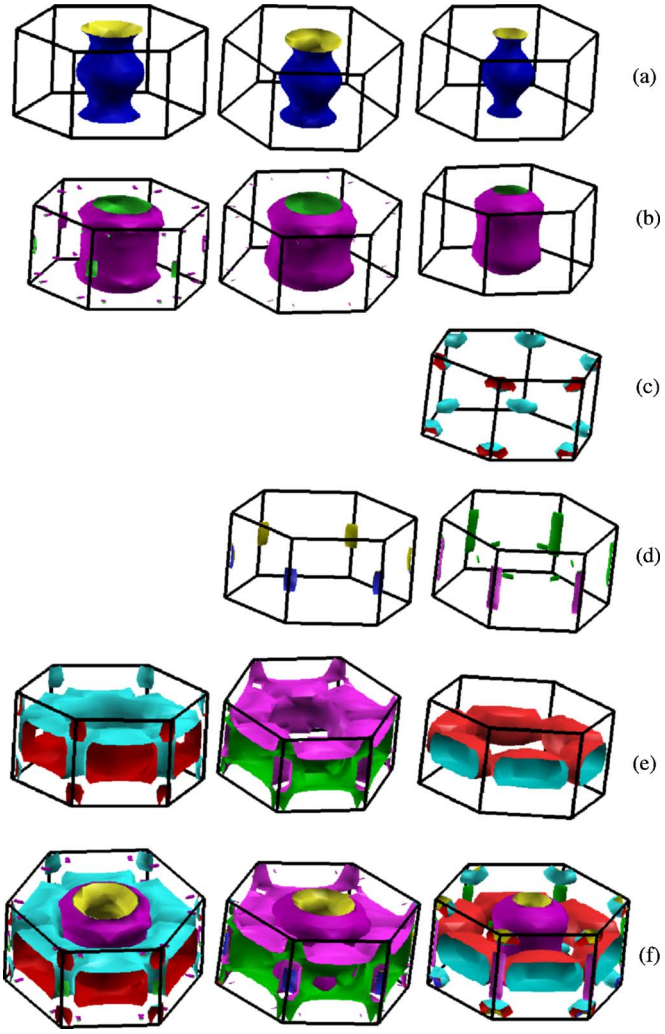

FIG. 6. (Color online) Three-dimensional Fermi surface per spin of gadolinium calculated, respectively, in GGA+SOC (left column), GGA (middle column), and GGA+U (right column) methods. (a), (b), and (c) represent the majority spin Fermi surfaces, the (d) and (e) the spin minority and (f) the total Fermi surface.

shown that within the LSDA (GGA), the f states strongly prefer the AFM order, whereas the p and d states prefer the FM order, and concluded that this is due to the unphysical partial occupation of the minority $4f$ states. Using the LDA (GGA)+U and, thus, removing the emphasized unphysical partial occupation of the $4f$ states, our calculations provide the correct experimental FM order. Our results are also in qualitative agreement with the results of Ref. 12. Thus, our calculation supports the fact that the force theorem, developed by Andersen and co-workers,[33] which was initially used to provide an analytical expression for the hydrostatic pressure of materials, works quite well for producing the total-energy differences between different magnetic configurations.

IV. XAS AND XMCD RESULTS

With the rapid evolution of the techniques of x-ray spectroscopy from the early days, particularly those of the

TABLE I. Calculated Fermi surfaces areas in a.u.$^{-2}$ within the GGA, GGA+SOC, GGA+U, and GGA+U+SOC. Notice that for the calculations with spin-orbit coupling, the spin is not a good quantum number and therefore there is a small spin mixing in all the bands.

	10 down	11 down	12 down	25 up	26 up	27 up
GGA	0.109	3.157	0.018	0.710	1.258	0.000
GGA+U	0.242	1.895	0.000	0.522	0.908	0.590
GGA+SOC	0.000	2.903	0.000	0.792	1.393	0.000
GGA+U+SOC	0.000	2.290	0.000	0.618	1.319	0.000

XMCD, and the progress achieved by the derivation of the XMCD sum rules,[34] it becomes possible to experimentally determine both the orbital and spin moments of each atomic species and orbital of a complex magnetic material. During the last decade, experimental studies have given rise to a huge amount of XMCD spectra of rare-earth magnetic materials, which are still incompletely understood and where only model calculations with many *ad hoc* parameters have been attempted so far.[35] Therefore the description of the microscopic interactions at play between matter and the exciting x-ray radiation by means of *ab initio* methods is of crucial importance. For this reason we have implemented x-ray absorption and XMCD within the FLAPW framework as in Refs. 36 and 37, in the FLEUR code, using the dipolar approximation, and applied it to the $L_{2,3}$ and $M_{4,5}$ edges of gadolinium.

A. $L_{2,3}$ edges

In this section we compare our calculated $L_{2,3}$ x-ray absorption spectra and XMCD spectra with previous calculated and experimental spectra. We denote by μ^+, μ^-, and μ_0 the absorption coefficients for right $(x+iy)$, left $(x-iy)$, and z-polarized x-ray radiation, respectively. In polar geometry where the magnetization direction is parallel to the wave vector of the x-ray beam, XMCD is defined as the difference between the absorption coefficients for right and left circular polarized x-ray radiation $\Delta\mu=\mu^+-\mu^-$, and the total absorption (XAS) is the average of μ^+, μ^-, and μ_0.

The calculated cross sections of the $L_{2,3}$ absorption coefficients, which involve an electronic transition from the $2p_{1/2}$ (L_2) and $2p_{3/2}$ (L_3) core levels towards the $5d$ and $6s$ unoccupied conduction states, are presented in Fig. 7 together with the experimental spectra obtained by Shütz and co-workers.[38] The calculated and experimental spectra are aligned so that the main structure has the same height and energy position as the experimental one. This is because the difference between the core-electron levels and the conduction states is not accurate within density functional theory (DFT). In fact, the core electrons are dominated by the exchange interaction and are therefore well described within a Hartree-Fock (HF) formalism, while the conduction electrons are usually well described within the DFT and not the HF formalism. The calculated spectra are also broadened using a Gaussian of full width at half maximum of 2.5 eV to account mainly for the lifetime of the $2p_{1/2}$ or $2p_{3/2}$ core hole. The results are in quite good agreement with the experimental spectra and are due to the good quality of the FLAPW eigenvalues and eigenvectors. It is interesting to note that our results are also slightly better than the previous results of Carra *et al.*,[17] even though they have included the quadripolar contribution. Our calculation seems to indirectly indicate that the quadripolar contribution is negligible compared to the dipolar one. Notice also that the Hubbard inter-

TABLE II. Total-energy difference between the AFM ($\uparrow\downarrow$) and the FM ($\uparrow\uparrow$) configurations using different approximations to the exchange and correlation all-electron potential.

	LSDA	LDA+U	GGA	GGA+U
$\Delta E_{(\uparrow\downarrow-\uparrow\uparrow)}$ (meV)	−24.48	78.62	−20.00	70.93

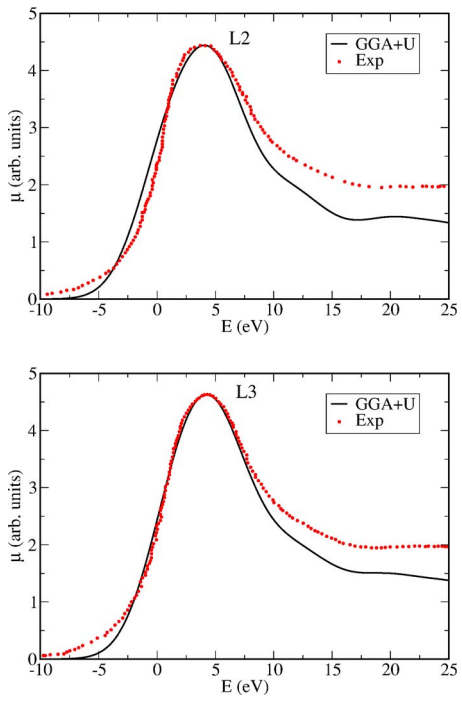

FIG. 7. (Color online) The upper and lower panels represent, respectively, the calculated L_2 and L_3 XAS (solid black curves) compared to the experimental ones (Refs. 38). The experimental curves are represented by red dotted curves (gray dotted curves). Because it is not possible to compare the absolute energy scale with respect to the $2p$ core level, the calculated and experimental spectra are aligned so that the maximum of the spectra has the same height and is at the same photon energy. The theoretical spectra are broadened using Gaussian of full width at half maximum of 2.5 eV.

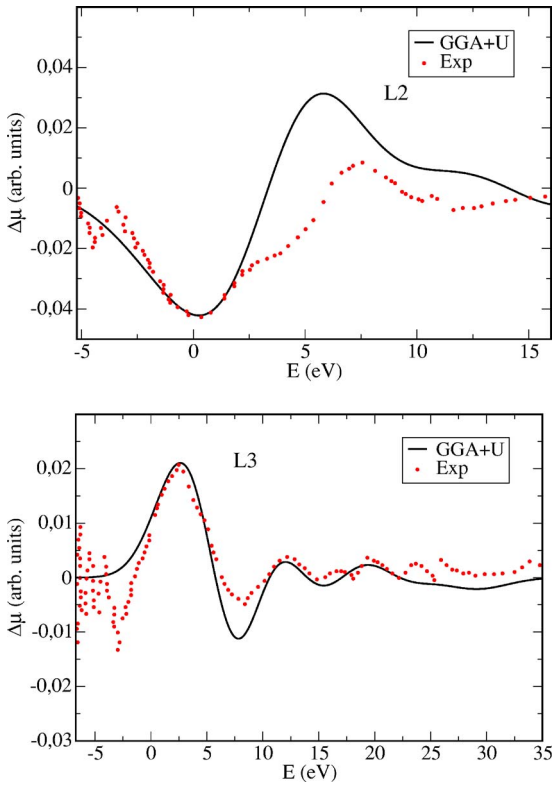

FIG. 8. (Color online) The upper and lower panels represent, respectively, the calculated L_2 and L_3 XMCD spectra (solid black curves) compared to the experimental ones (Ref. 38). The experimental curves are represented by dotted red curves (dotted gray curves).

action, although it provides the correct energy splitting between the occupied and the empty $4f$ states, it has very little effect on the shape of the L_2 and L_3 spectra.

Figure 8 shows the calculated L_2 and L_3 XMCD spectra (solid black curves) compared to the experimental ones.[38] Despite the visible difference between the calculated and the experimental positions of the peak at about 5 eV, the shape of the spectrum compares well with the experimental one.[38] We have also to mention that all the XMCD investigations have been carried out using the LSDA, LDA+U, GGA, and GGA+U potentials, and it turns out that regardless of the form of the potential, the shape of our spectra does not change appreciably. This is due to the fact that the deep occupied initial core states ($2p$ states) and the shape of the final $5d$ unoccupied DOS part of the involved electronic transitions are mostly the same for the different potentials despite the change in their energy positions.

B. $M_{4,5}$ edges

In this section we discuss the $M_{4,5}$ edges of gadolinium involving the M_4 ($3d_{3/2} \rightarrow 4f$) and the M_5 ($3d_{5/2} \rightarrow 4f$) transitions.

To study the $M_{4,5}$ edges of gadolinium we have calculated the x-ray right circularly polarized $M_{4,5}$ absorption spectra for every photon energy. Figure 9 compares our $M_{4,5}$ edges of gadolinium results for right circular polarization with the

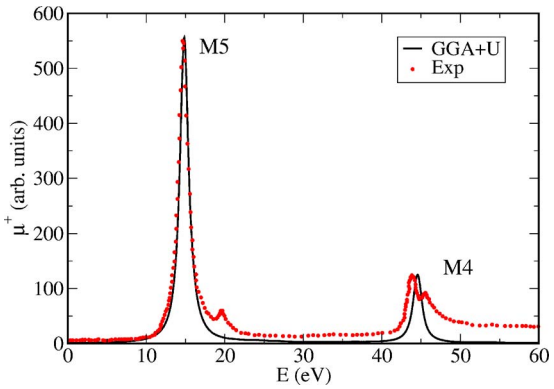

FIG. 9. (Color online) The $M_{4,5}$ calculated XAS (solid black curve) compared to the experimental one.[39] The experimental curve is represented by a dotted red curve (dotted gray curve). Because it is not possible to compare the absolute energy scale with respect to the $3d$ core level, the calculated and experimental spectra are aligned so that the structure with a maximum at around 15 eV has the same height and energy position as the experimental one. The calculated spectra are broadened using a Lorentzian of full width at half maximum of 1.1 eV.

corresponding experimental one of Ref. 39. The calculated and experimental spectra are aligned so that the structure with a maximum at around 15 eV has the same height and energy position as the experimental one. This is because, as stated earlier in the case of the $L_{2,3}$ edges, it is not possible to determine accurately the energy difference between the core levels and the conduction states. The calculated spectra are also broadened using a Lorentzian of full width at half maximum of 1.1 eV to account for the life time of the $3d$ core hole. Although our results show a branching ratio in good agreement with the experimental one, the experimental small structure located after the principal peak of M_5 and M_4 is not reproduced by our calculation. Our analysis showed that these structures are not accounted for by the ($3d_{3/2} \rightarrow 6p$) and ($3d_{5/2} \rightarrow 6p$) electronic transitions allowed by the dipolar selection rule $\Delta l = \pm 1$ because of the small amount of unoccupied $6p$ states present above the Fermi level. Indeed a separation of the two contributions $3d \rightarrow 4f$ and $3d \rightarrow 6p$ to the M_4 and M_5 spectra indicates that the latter is marginal with respect to the former, and it is not in any case as visible as it is in the experimental situation. Thus, these small structures do not arise from the one-electron electronic structure as is described in our first-principles (time-independent) scheme, but rather from dynamical interaction processes creating photoelectron core-hole interactions.

In Fig. 10 we have plotted our M_5 XMCD spectrum and that of Ref. 40 experimental work, as defined by

$$\Delta\mu = \mu^{+}_{M_5} - \mu^{-}_{M_5}. \tag{11}$$

We find in Fig. 10 again the experimental structures emphasized above. In their work Hu *et al.*[40] argued that in addition to the *direct* electric dipole transition (the pronounced M_4 and M_5 peaks), there is an *indirect channel* along which the same total final state can be reached via two *intermediate* processes. The first one is also of dipolar kind and consists of

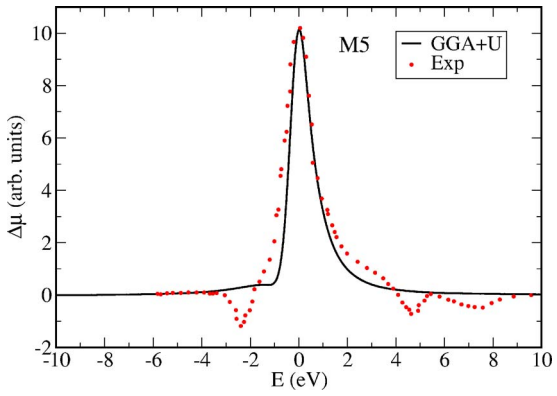

FIG. 10. (Color online) XMCD M_5 calculated spectrum (solid black curve) compared to the M_5 experimental one of Ref. 39. The experimental curve is represented by a dotted red curve (dotted gray curve). The intensities are in arbitrary units; the height of the structure at zero energy is aligned to the experimental one.

populating nd-hole state ($n=3$ or 4); the second one is of Coster-Kronig Auger recombination. This explanation confirms that our calculations reproduce only the dipolar part of the absorption coefficients. Even though our calculated spectra do not reproduce the overall experimental spectra, because they contain the extrinsic behavior of some transitions produced during the experimental probes, our calculated spectra allowed a distinction between the dipolar contribution part as an intrinsic behavior to the electronic structure and that of the extrinsic one lying beyond the scope of our investigation.

C. XMCD sum rules

In order to calculate the spin magnetic moment which comes mostly from the half-filled $4f$ shell ($S=7/2$, $L=0$) and $5d$ states we have applied the XMCD spin moment sum rule[34] to the $L_{2,3}$ and $M_{4,5}$ edges of gadolinium.[41] To illustrate the use of the sum rule, we give here the sum-rule spin moment for the $4f$ states:

$$\int_{E_F}^{E_{cut}} \left[(\mu^+_{M_5} - \mu^-_{M_5}) - \frac{3}{2}(\mu^+_{M_4} - \mu^-_{M_4}) \right] dE = \frac{N}{3N_h}(\langle \sigma_z \rangle + 6\langle T_z \rangle), \tag{12}$$

where

$$N = \sum_{\lambda=+,-,0} \int_{E_c}^{E_{cut}} (\mu^\lambda_{M_4} + \mu^\lambda_{M_5}) dE.$$

Here, $\langle \sigma_z \rangle$ is the expectation value of the spin moment and $\langle T_z \rangle$ the magnetic dipole term. The integrations are from the Fermi level energy E_F to the energy cutoff E_{cut}, which we took at 5 eV above the Fermi level, where the f density of states becomes almost zero. The number of f holes, N_h, has been deduced from the self-consistent integrated DOS of the unoccupied $4f$ density of states. Table III presents the calculated number of holes, N_h, the muffin-tin total spin magnetic moment, the d and f spin magnetic moments contributions to the muffin-tin one, the total magnetic moment (including the contribution of the interstitial region), and the orbital magnetic moment. The magnetic dipole term T_z which measures the asphericity of the spin magnetization is found to be of $(-0.031 \pm 0.002)\mu_B$ using the different types of potentials, and it essentially comes from the $5d$ states. The contribution of the $4f$ states is found to be zero in good agreement with the analytical expression, as at half filling the total spin momentum S is equal to the total momentum J.[34] The spin magnetic moment of $4f$ states can be calculated from Eq. (12) without the T_z term whereas it is important to include it for the determination of the $5d$ spin moment. Note that despite the tiny value of the expectation value of T_z, its contribution of $7\langle T_z \rangle$ to the $5d$ spin moment is large. In order to confront the XMCD results to the SC one, we have reported between parentheses in the same table the spin magnetic and the orbital moment calculated from the XMCD sum rules. The orbital moment of the $4f$ states is zero because $L=0$, but that of the $5d$ states is not. Since XMCD involves only electronic transitions in the muffin-tin region, the resulting sum-rule spin magnetic moment should be that of the corresponding

TABLE III. The first column contains the number of holes, N_h; the next five columns contain the spin magnetic moments μ_{mt} in the muffin-tin sphere, its d contribution μ_d and f contribution μ_f, the total magnetic moment μ_{tot}, and the orbital magnetic moment $\langle l_z \rangle$ for the $5d$ states. The XMCD sum-rule results are shown between parentheses, and the experimental magnetic moment is from Ref. 32.

	N_h	$\mu_{mt}(\mu_B)$	$\mu_d(\mu_B)$	$\mu_f(\mu_B)$	$\mu_{tot}(\mu_B)$	$\langle l_z \rangle(\mu_B)$
LSDA	6.76	7.12	0.32 (0.37)	6.74 (6.53)	7.48	−0.03 (−0.02)
LDA+U	6.89	7.38	0.38 (0.33)	6.94 (6.55)	7.78	−0.04 (−0.04)
GGA	6.89	7.18	0.33 (0.40)	6.78 (6.73)	7.58	−0.03 (−0.03)
GGA+U	6.94	7.37	0.38 (0.34)	6.94 (6.80)	7.77	−0.03 (−0.04)
Other theories					7.71,[a] 7.72[b]	
Expt.					7.63[c]	

[a]Reference 8.
[b]Reference 42.
[c]Reference 32.

muffin-tin sphere. From Table III we notice that the sum-rule spin magnetic moments are closer to the self-consistent (SC) f magnetic moments than to the total muffin-tin ones. As we have discussed above, our $M_{4,5}$ XMCD spectra are mostly of $3d_{3/2} \rightarrow 4f$ and $3d_{5/2} \rightarrow 4f$ because those of $3d \rightarrow 6p$ (which are also allowed by the dipolar selection rule) are negligible, and therefore the sum-rule spin magnetic moment is predominantly of f character. Thus, to be consistent we have to compare our sum-rule magnetic moment to the SC f magnetic moment rather than to the muffin-tin magnetic moment. The sum-rule magnetic moments are in good agreement with the SC f magnetic moment (the deviation is at most of 6%) regardless of the potential used; because—as previously stated—the potential choice does not affect the overall shape of the spectra or its integral, and hence the sum-rules magnetic moment is almost the same. For the $5d$ spin moments, the errors concerning the direct calculation and that of the sum rule are much larger in relative magnitude because these moments are much smaller compared to the $4f$ moments. However, for the $5d$ orbital moment the agreement seems much better between the two types of calculations. The disagreement in the case of the spin moments could be due to many factors, including inaccuracy in the evaluation of the T_z expectation value and/or to the fact that the XMCD sum rules are derived with severe approximations.

These results confirm that the T_z term in Eq. (12) is negligible. So it is not surprising that our SC calculations and sum-rule results (based on converged SC calculations) of the magnetic moment compare favorably with the experimental magnetic moment. According to Table III the total GGA +U magnetic moment of the SC calculations of $7.77\mu_B$ (of which the f magnetic moment is of $6.94\mu_B$ in good agreement with the sum-rule f magnetic moment of $6.80\mu_B$) is in good agreement with the experimental magnetic moment of $7.63\mu_B$ and with other calculations of Refs. 8 and 42.

It is therefore important to note that our XMCD spectra and the magnetic moment determined from the sum rules show the applicability, usefulness, and reliability of the sum rules for the determination of magnetic properties of strongly localized $4f$ rare-earth electrons and encourage further XMCD experimental studies of gadolinium or compounds containing gadolinium.

V. CONCLUSION

In conclusion, we have carried out self-consistent LSDA, GGA, LDA+U, and GGA+U first-principles FLAPW calculations of the electronic structure, x-ray absorption spectra, and XMCD of metallic gadolinium. Our electronic structure explorations provided the optimal U parameter (U=7.7 eV) that allowed the GGA+U and LDA+U methods to describe correctly both the experimental XPS and BIS. The LDA +U and GGA+U methods were able also to provide the correct magnetic configuration of gadolinium. Both LDA +U and GGA+U produced smaller Fermi surface areas than the LDA or GGA methods. This could motivate further first-principles calculations of the other physical properties of gadolinium or related compounds using either the GGA+U or LDA+U.

We have shown that the dipolar electronic transitions describe both the XAS and XMCD at the L_2 and L_3 edges in good agreement with the experimental spectra.[38] On the other hand, it was shown that for XAS and XMCD at the $M_{4,5}$ edges the agreement is only semiquantitative. Despite the good description of the XAS branching ratio, the upper small structure above the principal peak is missing in our calculation. This structure is due to multiplet effects not being taken into account in our *ab initio* calculation. Nevertheless, our XMCD investigation of metallic gadolinium shows the usefulness of the sum rules to characterize the magnetic properties of the strongly localized $4f$ electron.

ACKNOWLEDGMENTS

We gratefully acknowledge S. Blügel and G. Bihlmayer for supplying the FLEUR code, and useful discussions one of us (S.A.) had with them during his stay in Jülich. The calculations were performed using the SGI Intel supercomputer of the Université Louis Pasteur de Strasbourg and the IBM SP4 supercomputer of the CINES under computer Grant No. gem1100.

[1] J. O. de Dimmock and A. J. Freeman, Phys. Rev. Lett. **13**, 750 (1964).
[2] J. Sticht and J. Kübler, Solid State Commun. **53**, 529 (1985).
[3] W. Temmerman and P. A. Sterne, J. Phys.: Condens. Matter **2**, 5529 (1990).
[4] D. J. Singh, Phys. Rev. B **44**, 7451 (1991).
[5] P. G. Mattocks and R. C. Young, J. Phys. F: Met. Phys. **7**, 1219 (1977).
[6] J. E. Schirber, F. A. Schmidt, B. N. Harmon, and D. D. Koelling, Phys. Rev. B **16**, 3230 (1977).
[7] R. Ahuja, S. Auluck, B. Johansson, and M. S. S. Brooks, Phys. Rev. B **50**, 5147 (1994).
[8] C. Santos, W. Nolting, and V. Eyert, Phys. Rev. B **69**, 214412 (2004).
[9] Ph. Kurz, G. Bihlmayer, and S. Blügel, J. Phys.: Condens. Matter **14**, 6353 (2002).
[10] http://www.flapw.de
[11] A. B. Shick, A. I. Liechtenstein, and W. E. Pickett, Phys. Rev. B **60**, 10763 (1999).
[12] A. B. Shick, W. E. Pickett, and C. S. Fadley, Phys. Rev. B **61**, R9213 (2000).
[13] J. P. Perdew and A. Zunger, Phys. Rev. B **23**, 5048 (1981).
[14] S. V. Beiden, W. M. Temmerman, Z. Szotek, and G. A. Gehring, Phys. Rev. Lett. **79**, 3970 (1997).
[15] Z. Szotek, W. M. Temmerman, and H. Winter, Phys. Rev. B **47**, 4029 (1993).
[16] L. Petit, A. Svane, Z. Szotek, and W. M. Temmerman, Phys. Rev. B **72**, 205118 (2005).

[17] P. Carra, B. N. Harmon, B. T. Thole, M. Altarelli, and G. A. Sawatzky, Phys. Rev. Lett. **66**, 2495 (1991).
[18] M. Weinert, E. Wimmer, and A. J. Freeman, Phys. Rev. B **26**, 4571 (1982).
[19] E. Wimmer, H. Krakauer, M. Weinert, and A. J. Freeman, Phys. Rev. B **24**, 864 (1981).
[20] V. L. Moruzzi, J. F. Janak, and A. R. Williams, *Calculated Electronic Properties of Metals* (Pergamon, New York, 1978).
[21] J. P. Perdew, K. Burke, and M. Ernzerhof, Phys. Rev. Lett. **77**, 3865 (1996).
[22] A. I. Liechtenstein, V. I. Anisimov, and J. Zaanen, Phys. Rev. B **52**, R5467 (1995).
[23] O. Bengone, M. Alouani, P. Blöchl, and J. Hugel, Phys. Rev. B **62**, 16392 (2000).
[24] V. I. Anisimov and O. Gunnarsson, Phys. Rev. B **43**, 7570 (1991).
[25] J. R. Banister, S. Legvold, and F. H. Spedding, Phys. Rev. **94**, 1140 (1954).
[26] P. E. Blöchl, O. Jepsen, and O. K. Andersen, Phys. Rev. B **49**, 16223 (1994).
[27] D. Singh, Phys. Rev. B **43**, 6388 (1991).
[28] B. N. Harmon and A. J. Freeman, Phys. Rev. B **10**, 1979 (1974).
[29] J. K. Lang, Y. Baer, and P. A. Cox, J. Phys. F: Met. Phys. **11**, 121 (1981).
[30] A. J. Freeman, *Magnetic Properties of Rare-Earth Metals*, edited by R. J. Elliott (Plenum, London, 1972), Chap. 6.
[31] K. Maiti, M. C. Malagoli, E. Magnano, A. Dallmeyer, and C. Carbone, Phys. Rev. Lett. **86**, 2846 (2001).
[32] J. Jensen and A. R. Mackintosh, *Rare Earth Magnetism* (Clarendon Press, Oxford, 1991).
[33] H. Skriver, *The Lmto Method* (Spinger-Verlag, Berlin 1984).
[34] B. T. Thole, P. Carra, F. Sette, and G. van der Laan, Phys. Rev. Lett. **68**, 1943 (1992); P. Carra, B. T. Thole, M. Altarelli, and Xindong Wang, *ibid.* **70**, 694 (1993); see also A. Ankudinov and J. J. Rehr, Phys. Rev. B **51**, 1282 (1995).
[35] For a review see J. C. Parlebas, K. Asakura, I. Harada, and A. Kotani, Phys. Rep. **431**, 1 (2006).
[36] R. Wu, D. Wang, and A. J. Freeman, Phys. Rev. Lett. **71**, 3581 (1993).
[37] M. Alouani, J. M. Wills, and J. W. Wilkins, Phys. Rev. B **57**, 9502 (1998).
[38] G. Schütz, M. Knülle, R. Wienke, W. Wilhelm, W. Wagner, P. Kienle, and R. Frahm, Z. Phys. B: Condens. Matter **73**, 67 (1988).
[39] J. E. Prieto, F. Heigl, O. Krupin, G. Kaindl, and K. Starke, Phys. Rev. B **68**, 134453 (2003).
[40] Z. Hu, K. Starke, G. van der Laan, E. Navas, A. Bauer, E. Weschke, C. Schüssler-Langeheine, E. Arenholz, A. Mühlig, G. Kaindl, J. B. Goodkoep, and N. B. Brookes, Phys. Rev. B **59**, 9737 (1999).
[41] Note that we do not have to use the orbital moment sum rule because the $4f$ orbital moment is nul due to the fact that the spin-up states are fully occupied and the spin-down states are empty (total angular momentum is nul).
[42] A. Y. Perlov, S. V. Halilov, and H. Eschrig, Phys. Rev. B **61**, 4070 (2000).